

## Terahertz optical mixing in biased GaAs single quantum wells

V. Ciulin,\* S. G. Carter, and M. S. Sherwin

*iQUEST and Physics Department, University of California, Santa Barbara, California 93106, U.S.A*

A. Huntington and L. A. Coldren

*Materials Department, University of California, Santa Barbara, California 93106, U.S.A*

(Received 23 February 2004)

The nonlinear mixing of near-infrared (NIR) and terahertz (THz) laser beams is investigated experimentally in a square GaAs quantum well structure, where the symmetry of the sample can be controlled by applying an electric field along the growth direction. The mixing produces sidebands, which appear at  $\omega_{\text{sideband}} = \omega_{\text{NIR}} + n\omega_{\text{THz}}$ , where  $n = \pm 1, 2, \dots$ . For a given THz frequency, the intensity of the  $n = \pm 1$  sidebands displays two main resonances as a function of the NIR frequency. These resonances are separated by the THz frequency. Their intensity is found to depend strongly on the electric bias and on THz frequency. The  $n = \pm 1$  sideband intensity is zero when the sample is unbiased and increases significantly with bias. The sideband is strong when the THz laser frequency is tuned in resonance with an intersubband transition and also at low THz frequencies. The main features of our results are explained qualitatively, except at very high THz intensities, by a perturbative model of the nonlinear susceptibility  $\chi^{(|n|+1)}$ . At high THz intensities, the resonances are observed to red shift and broaden.

DOI: XXXX

PACS number(s): 78.67.De, 42.65.-k, 78.20.Jq

### I. INTRODUCTION

Electric fields affect the optical interband properties of semiconductors.<sup>1</sup> The effect is particularly strong in the quantum-confined Stark effect, when the field is applied along the growth direction of a quantum well (QW) sample. This allows efficient optical modulators and switches. Using high-frequency ac fields in the terahertz (THz) range is technologically interesting as demand grows for faster devices.<sup>2,3</sup> Fields in this energy range can furthermore couple conduction or valence subbands, allowing resonant effects. ac Stark effects have been predicted at high ac fields.<sup>4-6</sup>

In undoped QW's, the THz field can couple different excitonic states and thus modulate the interband (optical) polarization. This leads to changes in the exciton optical absorption and to the emission of sidebands at  $\omega_{\text{sideband}} = \omega_{\text{NIR}} + n\omega_{\text{THz}}$ , where  $\omega_{\text{NIR}}$  ( $\omega_{\text{THz}}$ ) is the frequency of the near infrared (THz) beam and  $n = \pm 1, \pm 2, \dots$ . There is a wealth of theoretical investigations predicting significant changes of the absorption under THz illumination and of sideband generation.<sup>5,7-10</sup> Previous experimental studies, in which the THz field was oriented in the QW plane, have reported small changes in absorption under a strong THz field<sup>11</sup> and even ( $n=2, 4, \dots$ ) sideband generation.<sup>12</sup> To generate odd sidebands, especially the efficient  $n=1$ , asymmetric coupled QW structures have been used with the ac electric field polarized in the growth direction of the QW.<sup>3,13</sup> In these structures, the intersubband spacings can be tuned by a dc bias.<sup>14</sup> For weak THz fields, some sideband properties were explained by a  $\chi^{(|n|+1)}$  nonlinear susceptibility model.<sup>12,15</sup> At high THz intensities nonperturbative theories have been found necessary.<sup>16</sup> Odd and even sidebands have been also observed in bulk GaAs.<sup>17</sup>

Here, we present a detailed study of the nonlinear mixing of a near-infrared (NIR) and THz laser beam in a square QW

structure. The THz electric field is oriented along the growth direction of the QW. To enhance the nonlinear mixing, the sample symmetry can be broken by applying a dc electric field along the growth direction. This model system has the advantage that the level of asymmetry can be controlled and that the resonances are well defined and much less numerous than in coupled QW's. In the present case, we can consider a three-state system including two heavy-hole excitonic levels and the ground state. The oscillator strength of the exciton is stronger than for coupled wells and it has been predicted that this configuration leads to very efficient sideband generation.<sup>9,18</sup> There are also several theoretical studies of THz electro-optic effects in square wells to which our results can be compared,<sup>5,19</sup> although the THz fields used theoretically are stronger than the ones achieved experimentally. We observe and study sidebands resulting from a three-wave ( $n = \pm 1$ ) and a four-wave ( $n = \pm 2$ ) mixing process. The  $n = 1$  sideband is zero in the absence of electric bias and grows approximately as the dc electric field squared. In contrast, the  $n=2$  sideband intensity changes little when a small dc bias is applied to the sample. For a given THz frequency, the  $n = \pm 1$  sideband typically exhibits two main resonances as the NIR frequency is varied: the resonances occur when the NIR frequency or the sum of NIR and THz frequencies is tuned to the lowest heavy-hole excitonic transition. The  $n = \pm 1$  sideband intensity is also found to depend on the THz frequency. It is strong when the THz pump is resonant with an intersubband transition and also at low THz frequencies when the THz pump is nonresonant. At medium THz field strength, our measurements can be qualitatively explained by a perturbative model of the nonlinear susceptibility  $\chi^{(|n|+1)}$ . This model is not adequate for stronger THz fields as the interband absorption strength and energy position are modified by the ac field.

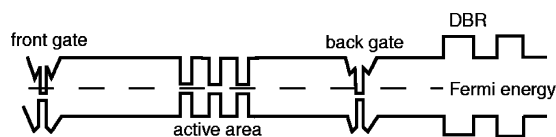


FIG. 1. Schematic diagram of the conduction band structure of the studied sample.

## II. SAMPLE AND EXPERIMENT

The samples are GaAs/AlGaAs heterostructures that consist of an active area, two gate QW's, and a 30-period 600-Å  $\text{Al}_{0.3}\text{Ga}_{0.7}\text{As}$  and 682-Å  $\text{Al}_{0.99}\text{Ga}_{0.01}\text{As}$   $\lambda_{\text{NIR}}/4$  distributed Bragg reflector (DBR). A schematic band diagram of the studied structure is shown in Fig. 1. The active area contains either a single or three 150-Å GaAs QW's separated by 300-Å  $\text{Al}_{0.3}\text{Ga}_{0.7}\text{As}$  barriers. Its center is situated close to a multiple of  $\lambda_{\text{NIR}}/2$  from both the sample surface and the DBR. Therefore the incident and reflected NIR laser beams interfere constructively at the center of the active area and the effective electric field of the NIR laser is enhanced. This leads to a peak absorption of the heavy-hole exciton larger than 50%, which is consistent with transfer matrix calculations.<sup>20</sup> The two gates, one on each side of the active area, are separated by about 1  $\mu\text{m}$ . They consist of 80-Å QW's with a  $\delta$ -doping layer 100 Å away. The distance between the DBR and the closest gate is 1600 Å.

The gates were contacted ohmically to allow applying a dc bias to the sample. To minimize potential electrical heating effects, the bias was turned on only when taking measurements with the THz source, which is on for about 5  $\mu\text{s}$  with a repetition rate of 1.5 Hz. The dc electric field was thus applied for 25  $\mu\text{s}$  and synchronized with each THz pulse. A piece of sapphire was mechanically pressed on the sample surface to form a waveguide for the THz in which the active area is close to the waveguide center. The two studied samples showed similar behavior and we restrict the present discussion to the sample with three QW's, as its sideband signal is stronger.

The sample's reflectivity spectrum is plotted in Fig. 2(a). The two peaks are the heavy-(hh1X) and light-(lhX) hole excitons. We will use the notation  $h m X$  for the heavy-hole exciton formed by an electron in the first conduction level and a hole in the  $m$ th level. When applying a bias, the hh1X and lhX spectral lines redshift as expected for the quantum confined Stark effect.<sup>1,22</sup> The change in energy with electric field, shown in Fig. 2(b), is strong for the hh1X. The graph is not totally symmetric around zero bias. An asymmetry is also observed in the current versus voltage curves not shown here. At negative bias, it appears that the maximum electric field achieved inside the sample is smaller than for positive bias: for  $V_{\text{bias}} < -1.6$  V the hh1X energy no longer changes. A possible explanation for this observation is interface roughness, since the GaAs/AlGaAs interface is poorer than the AlGaAs/GaAs one.<sup>23</sup> In addition, the intensity of the integrated photoluminescence (PL) was not constant for  $|V_{\text{bias}}| > \sim 2$  V, indicating the presence of disorder and/or charge transfer from the barrier or the gates into the QW. When an electric field is applied, the hh2X excitonic transi-

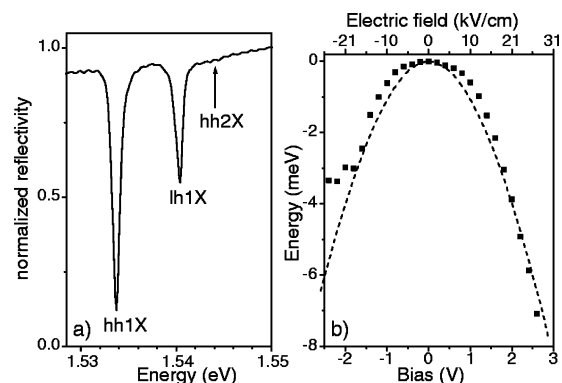


FIG. 2. (a) High-resolution normalized reflectivity spectra at 19 K and zero bias. The arrow indicates the spectral position of the hh2X transition that does not appear for unbiased structures. (b) Energy change of the hh1X reflectivity line as a function of bias and estimated electric field at 19 K, solid squares. The dashed line shows the result of our calculations (Ref. 21).

tion becomes possible and a peak appears at the energy indicated by the arrow in Fig. 2(a). The measured hh2X absorption was quite small (less than 1%) at around 0.5 V but was reliably measured using a differential technique that detects the change in the reflectivity when the bias is modulated.

Figure 3(a) shows the experimental configuration. For the measurements, the sample was held near 20 K in a closed-cycle helium cryostat. The THz beam was provided by the UCSB free electron laser<sup>24</sup> and was focused onto the cleaved edge of the sample by an off-axis parabolic mirror. The beam was on for 3–6  $\mu\text{s}$  at a repetition rate of 1.5 Hz. The THz laser power was measured before the sample with an electrically calibrated photothermophone energy meter (Thomas Keating Ltd.). To obtain the THz intensity, the spot size was measured by scanning a small aperture across the THz laser focus. The maximum intensity was found to be  $\sim 0.4 \text{ MW cm}^{-2}$  and the resulting estimated THz electric field inside the sample is  $\sim 9 \text{ kV/cm}$ . The polarization of the electric field of the THz laser was oriented along the growth direction of the sample, thus allowing coupling to intersubband transitions. The electron and light-hole intersubband

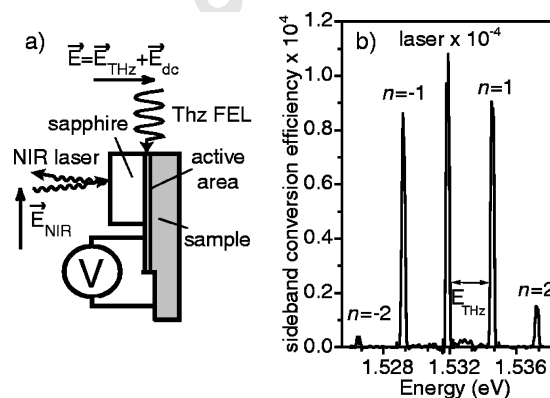


FIG. 3. (a) Schematic drawing of the experimental configuration. (b) Sideband spectra at 25 K for  $\hbar\omega_{\text{THz}} = 2.7$  meV with a bias  $V_{\text{bias}} = 1$  V and a THz laser intensity of  $\sim 0.1 \text{ MW cm}^{-2}$ .

transitions occur for energies larger than 40 meV and are out of reach of our THz source (0.5–20 meV). But the heavy-hole transition between the first two levels is around 10 meV and thus within the range of our source. The energy difference between the first heavy-hole and light-hole levels is around 6 meV. However, for small in-plane wave vectors, intersubband transitions between the heavy and light holes are weak.<sup>25</sup> Thus, in our model, we will consider only three levels: the ground state and the first and second heavy-hole excitons.

The NIR probe beam came from a tunable cw Ti-sapphire laser, which was chopped by an acousto-optic modulator into approximately 200  $\mu$ s pulses that overlapped each THz pulse. The NIR beam was reflected off the sample close to normal incidence and sent to a 0.85-m double monochromator, where it was detected by a photomultiplier tube. The NIR intensity on the sample was  $\sim 7$  W cm<sup>-2</sup>, yielding a total exciton density  $n_X \sim 10^{10}$  cm<sup>-2</sup> when the frequency is tuned in resonance with the hh1X transition. This excitation density is relatively high. Note, however, that the excitation density is lower when the NIR laser frequency is tuned away from the hh1X resonance. To verify that the high excitation density does not influence our observations significantly, measurements were also taken with an order-of-magnitude lower NIR intensity. The sideband resonances associated with the hh1X transition were narrower, but all trends were the same as those presented herein.

### III. EXPERIMENTAL OBSERVATIONS

Figure 3(b) shows a typical sideband spectrum. The central line is the NIR laser and the four surrounding peaks are the THz optical sidebands. They are separated from the main laser line by multiples of the THz frequency. The conversion efficiency from the NIR laser into the sidebands is here  $\sim 10^{-4}$ . This is comparable to the maximum conversion efficiency achieved in coupled QW samples with a similar number of QW's.<sup>14</sup> The intensity of the sideband in a given sample depends on several factors: (a) the NIR and THz laser frequencies with respect to the resonances, (b) the value of the dc electric field, and (c) the NIR and THz power. First, we will explore points (a) and (b) in the linear regime of THz power—i. e., where the  $n=1$  sideband intensity increases linearly with the THz intensity and the  $n=2$  increases quadratically.<sup>17</sup>

As the active region of the sample is very thin (<150 nm), the intensity of the sidebands is significant only close to the resonances of our system and the bulk contribution is not observable. Figure 4(a) presents sideband resonance scans obtained by measuring the sideband signal at  $\omega_{\text{NIR}} + n\omega_{\text{THz}}$  for  $n=-1$ , while scanning the NIR frequency. The spectra display a peak when the NIR frequency is close to the hh1X exciton transition. A second peak, higher in energy, appears when the sum of the NIR and THz frequencies is resonant with the hh1X. Therefore, the two peaks in the  $n=-1$  sideband resonance spectra are separated by  $\omega_{\text{THz}}$  as shown in the inset of Fig. 4(a). Schematic drawings of the transitions are shown in Fig. 4(b). Other resonances can occur that involve the hh2X level but they were not clearly

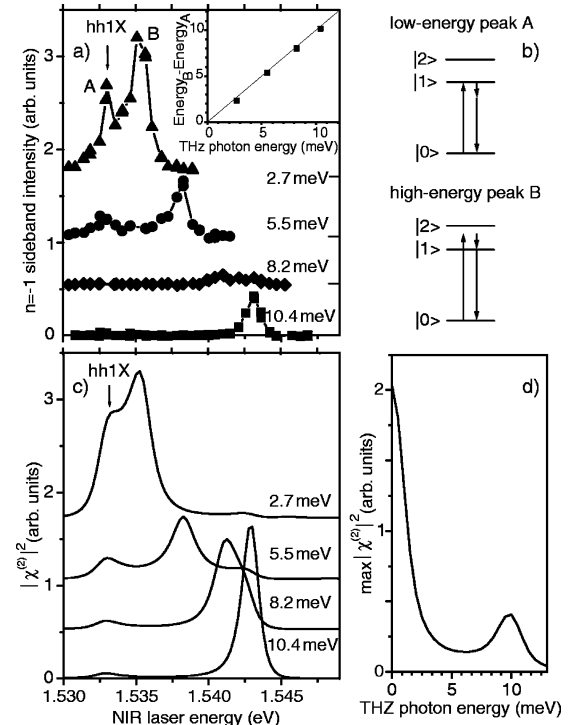


FIG. 4. (a) Sideband resonance spectra, showing the  $n=-1$  sideband intensity as a function of the NIR laser energy. The measurements were taken at 25 K and  $V_{\text{bias}}=1$  V ( $E_{\text{dc}}=10$  kV/cm) for  $\hbar\omega_{\text{THz}}=2.7$  (triangles), 5.5 (circles), 8.2 (diamonds), and 10.4 (squares) meV and THz laser intensities of  $\sim 25, 30, 40,$  and  $55$  kW cm<sup>-2</sup>, respectively (Ref. 26). The spectra have been offset for clarity. For each curve the offset is shown by a small line on the right side of the panel. Inset: energy difference between the two resonances labeled A and B as a function of  $\hbar\omega_{\text{THz}}$ . The line shows the predicted one-to-one-correspondence. (b) Schematic level model of the different transitions. (c)  $|\chi^{(2)}|^2$  calculated using Eq. (1) for the  $\hbar\omega_{\text{THz}}$  and  $E_{\text{dc}}$  used experimentally (Ref. 21). For the numerical evaluation of the plotted curves, we used  $\gamma=1$  meV and a GaAs band gap of 1.52 eV. (d) Calculated maximum of  $|\chi^{(2)}|^2(\omega_{\text{NIR}})$  as a function of  $\omega_{\text{THz}}$ .

seen experimentally. The  $n=1$  sideband spectra also show two peaks, as seen in Fig. 5(a), which arise from transitions similar to those presented in Fig. 4(b). For  $n=2$ , the sideband is weak under the present experimental conditions and we observed only one resonance when  $\hbar\omega_{\text{NIR}}$  is close to the hh1X energy.

We were able to observe sidebands at all THz frequencies explored, which ranged from  $\hbar\omega_{\text{THz}}=2.7$  to 14.1 meV. As shown in Fig. 4(a), the maximum intensity of the  $n=\pm 1$  sideband spectra varied nonmonotonically as a function of  $\omega_{\text{THz}}$ . A peak in intensity is found for  $\hbar\omega_{\text{THz}} \cong 10$  meV, which is close to resonance with the hh1 to hh2 transition. However, stronger sidebands were observed at small THz frequencies, even though the THz excitation intensities were smaller. It should be noted that it is difficult to quantitatively compare the sideband intensities for different THz frequencies. Indeed, the sideband intensity depends not only on the intensity of the THz beam before it hits the sample, which is the value that we can measure, but also on the efficiency of the coupling into the edge of the sample. In a first approxi-

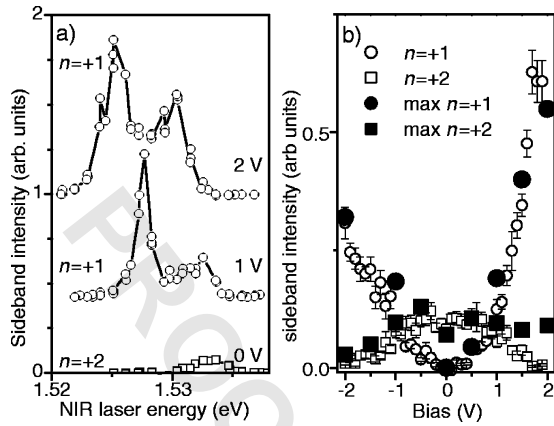


FIG. 5. (a) Sideband resonance spectra at 19 K with  $\hbar\omega_{\text{THz}} = 5.5$  meV and a THz laser intensity of  $\sim 30$  kW cm $^{-2}$ . The signal is detected at  $\omega_{\text{sideband}}$  as a function of the NIR laser energy. The  $n=2$  sideband intensity at  $V_{\text{bias}}=0$  V is shown with open squares and the  $n=1$  sideband with open circles at  $V_{\text{bias}}=1$  and 2 V. The spectra have been offset for clarity. (b) Intensity of the  $n=1$  (circles) and  $n=2$  (squares) sideband as a function of bias,  $V_{\text{bias}}$ , at  $\hbar\omega_{\text{NIR}} = 1.530$  and 1.5325 eV, respectively. The solid symbols show the peak intensity of the sideband resonance spectra when  $\omega_{\text{NIR}}$  is tuned to the hh1X energy.

mation, we neglect the effect of the waveguide as the NIR probe was close to the edge of the sample.

Figure 5 shows the intensity of the  $n=1$  and  $n=2$  sideband as a function of bias. The peaks are observed, Fig. 5(a), to shift towards the red with increasing bias. This is due mainly to the quantum confined Stark effect shown in Fig. 2(b). As the sideband resonance is broad around hh1X energy, we were able to measure the sideband intensity faithfully as a function of bias by sitting at a given NIR frequency, as seen in Fig. 5(b). The measurement at fixed NIR frequency is not as good for the  $n=2$  sideband, as shown by the deviation between the open and solid square symbols at positive bias. The  $n=1$  sideband intensity is zero for a square well and increases, roughly proportionally with  $E_{\text{dc}}^2$ , when the QW is biased and its symmetry is broken. The  $n=2$  sideband intensity is almost independent of bias for positive bias and decreases at negative bias. Figure 5(b) shows that the curves for the  $n=1$  and  $n=2$  are not symmetric around zero. An asymmetry between the positive and negative biases was also observed in the spectral properties without THz illumination in Fig. 2(b). We believe that these effects are linked and that the sideband properties are altered by interface roughness, disorder, and/or charge transfer. The measured dependence of the  $n=1$  and  $n=2$  sidebands with bias was qualitatively similar for all the THz frequencies used. However, from cool-down to cool-down, variations were observed for  $|V_{\text{bias}}| > 1.5$  V, and we also have measurements where the sidebands peak intensity decreases between 1.5 and 2 V. These changes are attributed to a degradation of the optical properties of the sample under strong dc electric field.

At high THz intensities, resonant coupling between subbands leading to the Autler-Townes splitting of the exciton absorption spectrum has been predicted.<sup>4</sup> Numerical calculations have been performed for a single quantum well, where

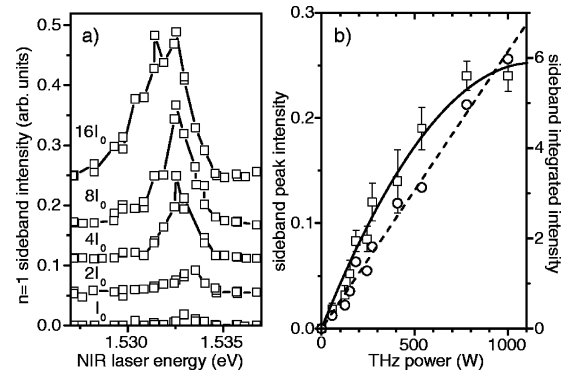


FIG. 6. (a)  $n=1$  sideband resonance spectra at 19 K with  $\hbar\omega_{\text{THz}} = 10.4$  meV and  $V_{\text{bias}} = 1$  V for different THz laser intensities. The max THz power is  $\sim 1$  kW. (b)  $n=1$  sideband peak (open squares) and integrated (open circles) intensity as a function of THz laser power. The lines are guides to the eyes.

the terahertz couples to the heavy-hole intersubband transition.<sup>5,19,27</sup> Experimentally, nonperturbative effects showing a saturation of the sideband intensity with the THz intensity have been reported in coupled QW's and in bulk GaAs.<sup>16,17</sup> Intense THz fields can dress the exciton states, and effects such as the Autler-Townes splitting are predicted to appear when the Rabi frequency  $\mu E_{\text{THz}}/\hbar$ , with  $\mu$  being the intersubband dipole moment, is larger than the dephasing rate. The necessary THz fields should be within our reach at the highest THz intensities. Figure 6 shows our experimental observations of the sideband resonance as a function of THz power. The maximum estimated THz intensity was  $\sim 0.2$  MW cm $^{-2}$  and the THz photon energy was 10.4 meV. The sideband resonance is observed to shift to the red and to broaden with increasing THz power. At higher THz intensity, the peak intensity of the  $n=1$  sidebands saturates. When plotting the integrated intensity of the  $n=1$  sideband, a linear power dependence is recovered. Thus the observed saturation in the sideband peak intensity comes here from broadening of the resonance under the THz field. A broadening of the resonance could be the first sign of the Autler-Townes splitting, when the THz pump is tuned to the heavy-hole transition as is the case experimentally. When the THz pump is out of resonance with the heavy-hole transition, theoretical calculations predict that the optical spectrum is affected in a different way.<sup>5</sup> Broadening of the sideband resonances was also observed with  $\hbar\omega_{\text{THz}} = 6.3$  meV, making an assignment of our observations to the Autler-Townes splitting possible but unlikely. Lattice heating by the THz beam can be in part responsible for the observed sideband broadening and redshift. However, this cannot be the only effect as the value of the redshift implies a much smaller increase in the lattice temperature than the broadening. A small in-plane component of the THz field could also contribute to a part of the observed redshift and broadening. Such a component may arise because of focusing and coupling into the modes of the dielectric waveguide of which the sample is a part. It would not contribute directly to the  $n=\pm 1$  sideband generation but can affect the absorption spectra.<sup>11</sup> Further experimental and theoretical studies are needed to elucidate the exact origin of our observations at high THz fields.

#### IV. MODEL AND DISCUSSION

With the exception of the observed saturation at high THz intensities, our results can be qualitatively explained by calculating the nonlinear optical susceptibility  $\chi^{(n|+1)}$ . We consider only three levels: the ground state, hh1X, and hh2X. The intensity of the  $n=1$  sideband is proportional to  $|\chi^{(2)}|^2 |E_{\text{NIR}}^x|^2 |E_{\text{THz}}^z|^2$  with<sup>28</sup>

$$\chi^{(2)}(\omega_{\text{NIR}} + \omega_{\text{THz}}, \omega_{\text{NIR}}, \omega_{\text{THz}}) \propto \sum_{m\nu} \frac{\mu_{0m}^x \mu_{m\nu}^z \mu_{\nu 0}^x}{(\omega_{m0} - \omega_{\text{NIR}} - \omega_{\text{THz}} - i\gamma_{m0})(\omega_{\nu 0} - \omega_{\text{NIR}} - i\gamma_{\nu 0})}, \quad (1)$$

where 0 is the ground state and  $m, \nu=1, 2$  are indices of the two heavy-hole exciton states considered, the hh1X and hh2X, respectively. In Eq. (1), some nonresonant terms that are very small have been ignored.  $\gamma$  is a measure of the linewidth of the transition. In the numerical evaluation of Eq. (1), a fixed value of 1 meV was used.  $\mu^x$  and  $\mu^z$  are the interband and intersubband matrix elements, respectively.  $\mu^x$  is proportional to the overlap of the electron and hole wave function of the transition.  $\mu^z$  is evaluated as

$$\mu_{m\nu}^z \propto \langle \Psi_{h\nu} | z | \Psi_{h_m} \rangle - \langle \Psi_{e_1} | z | \Psi_{e_1} \rangle \delta_{m\nu}. \quad (2)$$

The  $n=-1$  sideband intensity is proportional to Eq. (1) using a negative value for  $\omega_{\text{THz}}$ . The intensity of the  $n=\pm 2$  sideband is proportional to  $|\chi^{(3)}|^2 |E_{\text{NIR}}^x|^2 |E_{\text{THz}}^z|^4$ . The expression of  $\chi^{(3)}$  can be written analogously to Eq. (1).

The wave functions necessary to calculate the matrix elements in Eq. (1) are obtained by solving the Schrödinger equation numerically for electrons and holes in our QW as a function of the applied electric field.<sup>21</sup> To test our parameters, we have also variationally calculated the exciton binding energy:<sup>29</sup> the energy difference between the hh1X and hh2X of  $\sim 9.5$  meV and the change in hh1X exciton energy with electric bias agree fairly well with the measurements, as shown in Fig. 2. Using Eq. (1),  $|\chi^{(2)}|^2$  can be evaluated as a function of  $\omega_{\text{NIR}}$  for a given  $\omega_{\text{THz}}$ . The calculated curve has at least two peaks that correspond to the transitions described in Fig. 4. The energy position of these peaks matches the measurements well.

The intensity of the calculated  $n=-1$  sideband resonant spectra depends strongly on  $\omega_{\text{THz}}$  as shown in Fig. 4(c). It follows a nonmonotonic behavior similarly to the experimental spectra in Fig. 4(a). Our calculations do not fully reproduce the relative intensity of the peaks in the measured sideband resonance spectra. Some of the calculated peaks appear broader than in the measured spectra. The calculated spectra were normalized so that for the lowest used THz frequency, the intensities of the calculated and measured spectrum are comparable. Under these conditions, the calculated spectra at the two largest THz frequencies show a stronger signal than the one observed experimentally. There are several differences between measurements and calculations that can explain this. In the model, we have considered a fixed value of  $\gamma$  when evaluating Eq. (1), but  $\gamma_{10}$  and  $\gamma_{20}$  are not necessarily equal. This can change the relative intensity of the two peaks in each sideband resonance spectra. Also, the matrix

elements used to evaluate  $|\chi^{(2)}|^2$  are calculated for a bare QW and do not take into account that the cavity formed by the DBR and the sample surface enhances the strength of the optical transitions selectively. This can modify the relative intensity of the sideband resonances as a function of  $\omega_{\text{THz}}$ . Using Eq. (1), we have calculated the maximum value of  $|\chi^{(2)}(\omega_{\text{NIR}})|^2$  as a function of  $\omega_{\text{THz}}$ . Figure 4(d) shows the result of these calculations as a function of  $\omega_{\text{THz}}$ . The predicted  $|\chi^{(2)}|^2$  displays a peak when  $\omega_{\text{THz}}$  is close to the hh1X to hh2X intersubband transition and a larger maximum when  $\omega_{\text{THz}}$  tends towards zero. Thus, the model reproduces our data qualitatively. In our calculations, the large maximum at small  $\omega_{\text{THz}}$  arises from the term in which  $m=\nu=1$ . This term involves only the hh1X and ground states and is small for large  $\omega_{\text{THz}}$ . It takes advantage of the large interband matrix element of hh1X, while the interband matrix element of hh2X is quite small. The sideband signal can be thought of as arising from the optical transition being quasistatically modulated. This effect can be stronger when the hh1X transition strength is enhanced by a cavity. Several studies have theoretically addressed the issue of nonresonant modulation with low THz frequencies.<sup>4,5,30</sup>

The model also predicts that the intensity of both peaks of the  $n=\pm 1$  sideband is zero for a square well and increases as the electric field breaks the sample symmetry. The calculated dependence of the intensity of the high-energy peak of  $n=1$  sideband has the shape of a parabola, centered at zero, but it saturates around  $|V_{\text{bias}}|=1.5$  V. At this voltage, the calculated overlap between the electron and hole wave functions decreased significantly with respect to the zero-bias value. In a similar way, we have calculated  $|\chi^{(3)}|^2$  to model the behavior of the  $n=2$  sideband. The peak intensity around the hh1X transition is predicted to stay almost constant until 1 V and then increase a little before decreasing at 1.5 V. Our calculations reproduce most of the experimentally observed features shown in Fig. 5. The  $n=1$  sideband intensity increases significantly for small applied biases while the  $n=2$  sideband intensity stays rather constant. Discrepancies between experiment and calculations occur at larger biases and the decrease in the sideband intensity predicted for  $|V_{\text{bias}}|>1.5$  V is not clearly observed experimentally. The latter could be masked by disorder and/or charge transfer related effects that modify the sample optical properties at large biases.

#### V. CONCLUSION

In conclusion, we have studied nonlinear THz electro-optical effects in single GaAs QW's, where the symmetry can be broken by applying a bias. We find that we can control the intensity of the  $n=\pm 1$  sideband by changing the applied bias and the frequency of the THz beam. At zero bias, the  $n=\pm 1$  sideband intensity is zero and it increases roughly quadratically with the applied dc electric field. The  $n=\pm 1$  sideband intensity also varies nonmonotonically with the frequency of the THz beam. It becomes particularly strong at low THz frequencies. With a careful sample design, this effect could be exploited for efficient wavelength con

version. Our results are explained qualitatively, except at very high THz intensities, by a perturbative model of the nonlinear susceptibility. The model also predicts that the sideband intensity can saturate at finite dc electric fields due to the decrease in overlap between the electron and hole wave functions. At high THz intensities, where strong changes to the absorption spectrum had been predicted,<sup>5</sup> the resonances are observed to shift in energy and broaden.

## ACKNOWLEDGMENTS

We are grateful for fruitful discussions with A. V. Maslov and D. S. Citrin. We thank A. V. Maslov for encouraging us in this study and for sharing unpublished high-THz-field calculations with us. We acknowledge support from NSF Grant No. DMR 0244390 and Sun Microsystems. V. C. thanks the Swiss NSF for additional support.

\*Present address: V. Birkedal née Ciulin, Department of Chemistry, University of Aarhus, Langelandsgade 140, DK-8000 Aarhus C, Denmark.

- <sup>1</sup>S. Schmitt-Rink, D. S. Chemla, and D. A. B. Miller, *Adv. Phys.* **38**, 89 (1989).
- <sup>2</sup>D. S. Citrin and S. Hughes, *Appl. Phys. Lett.* **78**, 1805 (2001).
- <sup>3</sup>S. G. Carter, V. Ciulin, M. S. Sherwin, M. Hanson, A. Huntington, L. C. Coldren, and A. C. Gossard, *Appl. Phys. Lett.* **84**, 840 (2004).
- <sup>4</sup>S. Autler and C. H. Townes, *Phys. Rev.* **100**, 703 (1955).
- <sup>5</sup>A. V. Maslov and D. S. Citrin, *Phys. Rev. B* **62**, 16 686 (2000).
- <sup>6</sup>A. Liu and C. Z. Ning, *J. Opt. Soc. Am. B* **17**, 433 (2000).
- <sup>7</sup>A. P. Jauho, and K. Johnsen, *Phys. Rev. Lett.* **76**, 4576 (1996).
- <sup>8</sup>D. S. Citrin, *Phys. Rev. B* **60**, 13695 (1999).
- <sup>9</sup>A. Shimizu, M. Kuwata-Gonokami, and H. Sakaki, *Appl. Phys. Lett.* **61**, 399 (1992).
- <sup>10</sup>C. J. Dent, B. N. Murdin, and I. Galbraith, *Phys. Rev. B* **67**, 165312 (2003).
- <sup>11</sup>K. B. Nordstrom, K. Johnsen, S. J. Allen, A.-P. Jauho, B. Birnir, J. Kono, T. Noda, H. Akiyama, and H. Sakaki, *Phys. Rev. Lett.* **81**, 457 (1998).
- <sup>12</sup>J. Cerne, J. Kono, T. Inoshita, M. Sherwin, M. Sundaram, and A. C. Gossard, *Appl. Phys. Lett.* **70**, 3543 (1997).
- <sup>13</sup>C. Phillips, M. Su, M. Sherwin, J. Ko, and L. Coldren, *Appl. Phys. Lett.* **75**, 2728 (1999).
- <sup>14</sup>M. Y. Su, S. G. Carter, M. S. Sherwin, A. Huntington, and L. A. Coldren, *Appl. Phys. Lett.* **81**, 1564 (2002).
- <sup>15</sup>M. Y. Su, C. Phillips, J. Ko, L. Coldren, and M. S. Sherwin, *Physica B* **272**, 438 (1999).
- <sup>16</sup>M. Y. Su, S. G. Carter, M. S. Sherwin, A. Huntington, and L. A. Coldren, *Phys. Rev. B* **67**, 125307 (2003).
- <sup>17</sup>M. A. Zudov, J. Kono, A. P. Mitchell, and A. H. Chin, *Phys. Rev. B* **64**, 121204(R) (2001).
- <sup>18</sup>A. V. Maslov and D. S. Citrin, *Solid State Commun.* **120**, 123 (2001).
- <sup>19</sup>A. V. Maslov and D. S. Citrin, *Phys. Rev. B* **64**, 155309 (2001).
- <sup>20</sup>V. Savona, L. Andreani, P. Schwendimann, and A. Quattropani, *Solid State Commun.* **93**, 733 (1995).
- <sup>21</sup>Calculation parameters for the numerical solution of Schrödinger's equation: electron mass,  $m_e=0.067$ ; hole mass,  $m_{h(z)}=0.48$ ; in-plane hole mass,  $m_{h(R)}=0.082$ . The band gap was split 60:40 between the conduction and valence bands.
- <sup>22</sup>E. E. Mendez, G. Bastard, L. L. Chang, L. Esaki, H. Morkoc, and R. Fischer, *Phys. Rev. B* **26**, 7101 (1982).
- <sup>23</sup>M. Naganuma, T. Ishibashi, and Y. Horikoshi, *J. Appl. Phys.* **62**, 644 (1987).
- <sup>24</sup>G. Ramian, *Nucl. Instrum. Methods Phys. Res. A* **318**, 225 (1992).
- <sup>25</sup>F. Szmulowicz and G. J. Brown, *Phys. Rev. B* **51**, 13 203 (1995).
- <sup>26</sup>The sideband spectra shown are not corrected for the fact that the THz pulse length is not the same at all  $\omega_{\text{THz}}$ . The shortest pulse occurred at  $\hbar\omega_{\text{THz}}=2.7$  meV. Correcting for this effect would increase the sideband intensity at the lowest  $\omega_{\text{THz}}$  by less than a factor 2.
- <sup>27</sup>A. V. Maslov and D. S. Citrin, *IEEE J. Sel. Top. Quantum Electron.* **8**, 457 (2002).
- <sup>28</sup>R. W. Boyd, *Nonlinear Optics* (Academic Press, [REDACTED], 1992).
- <sup>29</sup>D. A. B. Miller, D. S. Chemla, T. C. Damen, A. C. Gossard, W. Wiegmann, T. H. Wood, and C. A. Burrus, *Phys. Rev. B* **32**, 1043 (1985).
- <sup>30</sup>D. S. Citrin and W. Harshawardhan, *Phys. Rev. B* **60**, 1759 (1999).